Supporting Information**:**

Decoding the Superlattice and Interface Structure of Truncate PbS Nanocrystal-Assembled Supercrystal and Associated Interaction Forces

Ruipeng Li [†], Kaifu Bian [#], Tobias Hanrath [#], William A. Bassett [Δ] and Zhongwu Wang [†*]

[†] Cornell High Energy Synchrotron Source, Wilson Laboratory; [#] School of Chemical and Biomolecular Engineering; and [Δ] Department of Earth and Planetary Science, Cornell University, Ithaca, New York 14853, USA.

1. Experimental:

A. Synthesis of truncated PbS nanocrystals (NCs):

Truncate PbS NCs were synthesized following the method reported by Hines and Scholes.[S1] In the synthesis, 0.45 g of lead oxide was dissolved in 20 mL of oleic acid to form lead oleate solution. The solution was heated to 150 °C and stirred for one hour under flowing nitrogen for degassing. Then, the solution was heated up to the injection temperature of 180 °C. In a glove box, 252 μL of bis(trimethylsilyl)sulfide (TMS) was dissolved in 12 mL of 1-octadecene (ODE) and stirred thoroughly. A 10 mL portion of the TMS solution was rapidly injected into the vigorously stirred and hot lead oleate solution. After injection and consequent indication of PbS NC formation, the solution turned to be brown immediately. The crude product

was collected after 1 min of the reaction, and then washed and size-selected by sequential precipitation with ethanol and re-dispersed in hexane. After the solvent was removed by blowing nitrogen, the dried NCs were stored inside a nitrogen glove box (oxygen <1 ppm) for additional physical processing. In addition, $Pb(OA)_2$ solids were freshly extracted during the NC synthesis before injecting sulfur precursor.

B. Assembly of truncate PbS NCs:

The truncate PbS NC-assembled supercrystals were grown from 0.1M PbS suspensions of hexane. The vials were sealed properly to maintain a slow evaporation rate without interruption for NC assembly. The NC assembly process took about 10 days. The powder samples of NC supercrystals were made by drop-casting 0.1M PbS NC suspensions of hexane on Kapton tape in air.

C. Synchrotron Small/Wide angle X-ray scattering (SAXS/WAXS) measurements:

Both the SAXS and WAXS images of PbS NC-assembled supercrystals were collected at the B1 station, Cornell High Energy Synchrotron Source (CHESS). Incident white x-rays were converted to the monochromatic beam with a fixed energy of 25.514 keV, equivalent to x-ray wavelength of 0.485946 angstrom. The monochromatic x-rays were collimated using a double pinhole-aligned circular tube into small x-ray beam with a diameter of 100 microns. X-ray scattering signals from the samples were collected using a large area Mar345 detector. The sample-to-detector distance was optimized, allowing acceptable resolutions of both the SAXS

and WAXS collected simultaneously from the same volume of the samples. The sample-to-detector distance and other detector sitting parameters were calibrated using the two powder standards of Ag behanate and CeO_2 for SAXS and WAXS, respectively. The raw two dimensional (2D) images were either reduced into one dimensional patterns using the *Fit2D* package [S2] or directly used for structural characterization and analyses. The powder samples were kept on Kapton tape and loaded directly to the sample stage for collection of SAXS and WAXS images. The experimental procedure is the same as that described previously.

D. Electron microscopy characterizations:

The as-synthesized PbS NCs were prepared by drop-casting the dilute NC hexane suspensions onto carbon coated 200 mesh copper TEM grids for transmission electron microscopy (TEM) characterization. TEM images were taken using an FEI Tecnai T12 operated at 120kV. NC diameters were measured by statistics of at least 200 NCs observed in TEM images. The assembled supercrystals of PbS NCs were carefully transferred onto a Si wafer for scanning electron microscopy (SEM) imaging. SEM images with different magnifications were taken using a LEO 1550 FESEM operated at 5-10 kV.

E. High pressure measurements of NC supercrystals, oleic acid and $Pb(OA)_2$:

Three samples including NC supercrystal, oleic acid (OA) and lead oleate [$Pb(OA)_2$] were loaded into a diamond anvil cell (DAC) for separate *in-situ* high pressure SAXS runs. Stainless gaskets were pre-indented to reduce the thickness from 250 μm down to ~100 μm. A 200 μm

diameter hole was drilled and served as the sample chamber. The samples were loaded into the gasket hole and then several small ruby chips were randomly distributed on the top of the samples for monitoring pressure. A laser-excited ruby fluorescence technique was used to check the pressure change. There are slight differences in sample-loading: 1) PbS supercrystal was added with silicone oil as a pressure medium; but 2) OA and $Pb(OA)_2$ did not include any pressure medium. Incident x-rays were optimized at a fixed energy of 25.514 keV to illuminate the samples. The x-ray scattering signals from the samples were collected using a large area Mar345 detector. In order to avoid possible degradation, fresh $Pb(OA)_2$ samples were used for high pressure SAXS measurements. The calibration procedure and the data analyses are the same as described previously.

F. Simulations of single supercrystal WAXS patterns:

Single supercrystal model used for simulations of SAXS and WAX patterns was built and visualized using a VESTA3.1 package. [S3] Individual NC was created based on the galena (cubic rocksalt) structure with space group *Fm3m*. The truncated shape was generated from a 8x8x8 cubic unit cell. The corner atoms of the cube were cut off along the (111) plane, allowing exposure of eight PbS{111} and six PbS{100} facets. The NCs were assembled with identical orientations into *fcc* superlattice using the reconstruction process described below. The other shape-related pseudo-polymorphs of superlattice were reconstructed based on the first single supercrystal lattice by exchanging NCs at face-center sites. The lattice symmetry of each pseudo-polymorph was accordingly verified by program PLATON [S4]. The six shape-related

superlattice pseudo-polymorphs were analyzed and merged into the two non-degeneration polymorphs eventually. The details are described in the later section.

Simulations of single supercrystal diffraction images were performed using the two commercial packages of "CrystalMaker" and "SingleCrystal". Individual NC model was used to generate two-dimensional (2D) scattering images of single supercrystals with desired orientation.

G. Calculation of the OA packing densities at PbS{111} and PbS{100} surface facets.

To estimate the area packing density of OAs at PbS{111} and PbS{100} surface facets, we first calculated the upper limit of OA packing density based on the crystalline structure of PbS NCs. One lead oleate [$Pb(OA)_2$] can be simply described by one Pb atom bound to two OA molecules. At NC surfaces, previous studies indicate that only Pb atoms can be bound by OA molecules. If each Pb atom is bound by one OA molecule, the packing density of OAs was calculated as 6.55 OA/nm^2 at PbS{111} surface facets and 5.68 OA/nm^2 at PbS{100} surface facets, respectively. The calculation details are step-by-step described below:

1. The lattice constant of PbS nanocrystal is a = 5.942 Å.
2. The 2D unit cell at PbS{111} and PbS{100} surface facets contain 0.5 Pb atom in a triangle cell and 1 Pb atom in a square cell, respectively.
3. The 2D lattice constants at PbS{111} and PbS{100} surface facets are calculated by:

$$a_{\{111\}} = a \times \frac{\sqrt{2}}{2} = 4.202\text{Å}$$

$$a_{\{100\}} = a \times \frac{\sqrt{2}}{2} = 4.202\text{Å}$$

Accordingly, the unit sizes are given by:

$$S_{\{111\}} = a_{\{111\}}^2 \times \frac{\sqrt{3}}{4} = 7.605\text{Å}^2$$

$$S_{\{100\}} = a_{\{100\}}^2 = 17.564\text{Å}^2$$

4. The densities of OAs at PbS{111} and PbS{100} surface facets, if assuming that all Pb sites at surface facets are coated by OA molecules, are obtained:

$$\rho_{\{111\}} = \frac{Z_{\{111\}}}{S_{\{111\}}} = \frac{0.5}{7.605\text{Å}^2} = 6.55 nm^{-2}$$

$$\rho_{\{100\}} = \frac{Z_{\{100\}}}{S_{\{100\}}} = \frac{1}{17.564\text{Å}^2} = 5.68\ nm^{-2}$$

However, the OA packing density at NC surfaces cannot be larger than the packing density of 4.4 OA/nm^2 calculated from the ideal crystalline OA and Pb(OA)$_2$ phase. This means that a fraction of Pb atoms are barely exposed at NC surfaces. Note: the OA packing density was calculated from the lamellar structures of both OAs in α phase and Pb(OA)$_2$ phase. To allow for inter-penetration of OA molecules from two nearest neighboring NCs, the lower limit of the packing density should be 4.4/2=2.2 OA/nm^2, which means that one molecule is removed from each pair of neighboring OAs. Considering the preferred linkage of OA to Pb site, the fully overlapped OA molecules have a similar structure to the β phase of OAs. [S5]

The supercrystal lattice gives the inter-NC distance of 3.0 ~ 3.4 nm, implying that the OA molecules from two nearest neighboring NCs are partially inter-penetrated, so the OA packing density at NC surfaces should be lower than that of the crystalline phase of OA and Pb(OA)$_2$. In-situ high pressure SAXS studies revealed that the inter-NC distance of NC supercrystal reduces

much faster than the lamellar distance of pure molecular crystalline phases upon compression. To allow such a quick compression of OAs and intercalation, the neighboring distance between OAs should be around $\sqrt{2}$ times of the crystalline packing. The packing density could be estimated to be $4.4/\sqrt{2}$=3.1 OA/nm^2. The above consideration and analysis allow us to estimate the packing density of OAs at NC surfaces in a reasonable range of 2.1 and 3.1 OA/nm^2, which are in a fair agreement with the literatures. [S6]

Alternatively, we used the area density of Pb sites at surface {111} and {100} facets to estimate the area density of OAs at NC surfaces. As is calculated above, the Pb sites on {111} and {100} facets of NC surfaces are 6.55 and 5.68 Pb/nm^2, respectively. Based on the lattice parameters of pure oleic acid phase in α form, the area packing density of OA molecules across one monolayer was estimated to be 4.4 OA/nm^2. $Pb(OA)_2$ solid displays a similar lamellar structure that has a slightly longer lamellar distance than that in the α form of OAs. This difference is caused by one additional Pb atom in middle that connects two OA molecules to form a long molecule chain. Thus, it is reasonable to assume that both OA and $Pb(OA)_2$ have the same area OA packing density of 4.4 OA/nm^2. Based on these two lamellar structures, we propose the two OA binding models at NC surfaces: 1) binding of one OA to only one Pb site; and 2) binding of one OA to two Pb sites. In the first model, half of Pb sites are barely exposed at NC surfaces, leaving enough room for OA intercalation; but in the second model, Pb sites are fully covered, but the free spacing between neighboring OAs is apparently the same as that in the first model. This above models and consideration give the upper limit of 3.06 OA/nm^2. Obviously, the upper limit represents the ideal case, so it is reasonable to slightly reduce the Pb binding sites in which a reduced ratio of Pb sites are OA-bound, thus allowing us to estimate the

low limit of 2.04 OA/nm^2. Please see the calculation details and resulting datasets given in Table S4.

H. Calculation for inter-NC distance of NC Supercrystal:

In assembled supercrystal with a *fcc* lattice, the inter-NC distance can be calculated using the d-spacing of SL(111) from the SAXS measurements. Using the powder sample given in Figure 1 of the text, the details of the calculation procedure are step-by-step described below:

1. Based on the SAXS measurement, the d-spacing of SL(111) can be calculated as $d_{SL(111)}$ = 11.68 nm.
2. The unit cell constant can be obtained: $a = d_{SL(111)} \times \sqrt{3}$ = 20.23 nm.
3. The inter-NC distance ($d_{NC\text{-}NC}$): $d_{NC\text{-}NC} = a \times \sqrt{2}$ = 14.25 nm.
4. Given of NC size d_{NC} = 11.3 nm, the gap between two neighboring NCs: $d_{gap} = d_{NC\text{-}NC} - d_{NC}$ = 2.95 nm.

I. Reconstruction of the superlattice and NC orientation of supercrystal.

The reconstruction processes are based on a series of high quality synchrotron-based SAXS and WAXS images collected from single supercrystals along several typical crystallographic projections at CHESS. For SAXS, large grains of supercrystals make smaller of the reciprocal lattice, but unlike atoms that have exactly the same size, much larger NC building blocks always display a small distribution of particle size, accordingly leading to the appearance of additional SAXS peaks. On the other hand, the regular atomic crystals diffract x-rays with strict obey of

Bragg laws in wide angle region. In case of single crystal, only the crystalline planes projected on the flat detector plane can produce the WAXS spots. In addition, the unique scattering textures are due to the typical lattice orientation in parallel to x-rays. These components can allow us to determine the arrangements of NCs in typical superlattice planes defined by single supercrystal SAXS patterns.

Firstable, the SAXS images are used to determine the typical orientation of NC-assembled supercrystal that is parallel to x-rays. Then, using the symmetrical distributions of scattering spots on WAXS images collected from the same volume of single supercrystal grain, we are able to determine how truncate NCs arrange themselves at different crystallographic sites.

In addition, simulations of single supercrystal scattering images with different oriented NCs help to confirm the reliability of the reconstructions.

J. Determination and Degeneration of Shape-related Superlattice Pseudo-polymorphs.

The shape-related superlattice *pseudo*-polymorphs are derived in terms of distinct orientations of truncate NCs between various crystallographic sites of *fcc* lattice. Through position exchanging of NCs at three face-center sites, six superlattice pseudo-polymorphs are derived and shown in Figures S8(a, b). Taking into count the super lattice transformation and the equilibrant symmetries, the six superlattice pseudo-polymorphs are accordingly degenerated into two independent pseudo-polymorphs, which are shown in Figure 4 in text. For better understanding, Figures S8(c, d) show the details for the degeneration and transformation correlations between various pseudo-polymorphs: one polymorph shown in Figure S8c is

degenerated from two original pseudo-polymorphs; and the other one in Figure S8d is from four original pseudo-polymorphs.

Supporting References:

[S1] Hines, M.A.; Scholes, G. D. *Adv. Mater***. 2003**, 15**,** 1844-1849.

[S2] Hammersley, A.P., ESRF Internal Report, ESRF97HA02T, 1997.

[S3] Momma, K. Izumi, F. *J. Appl. Crystallogr*. **2011**, 44, 1272-1276.

[S4] Spek, A. L. *Acta Cryst.* **2009** D65, 148-155.

[S5] Kaneko, D.; Yamazaki, K.; Kitagawa, K.; Kikyo, T.; Kobayashi, M.; Kitagawa, Y.; Matsuura, Y.; Sato, K.; Suzuki, M. *J. Phys. Chem*. B **1997**, 101, 1803

[S6] Moreels, I.; Juaro, Y.; De Geyter, B.; Haustraete, K.; Martins, J. C.; Hens, Z *ACS Nano* **2011**, 5, 2004–2012.

2. Supporting Figures:

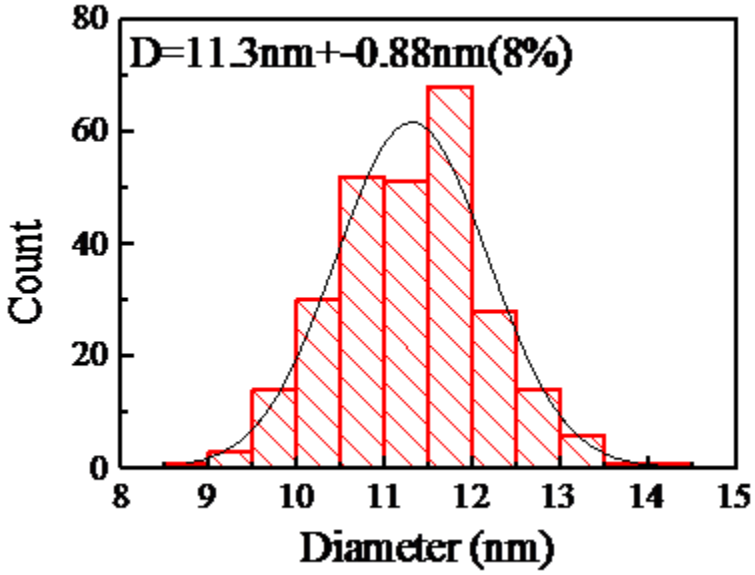

Figure S1 Size distribution of the synthesized PbS nanocrystals**.**

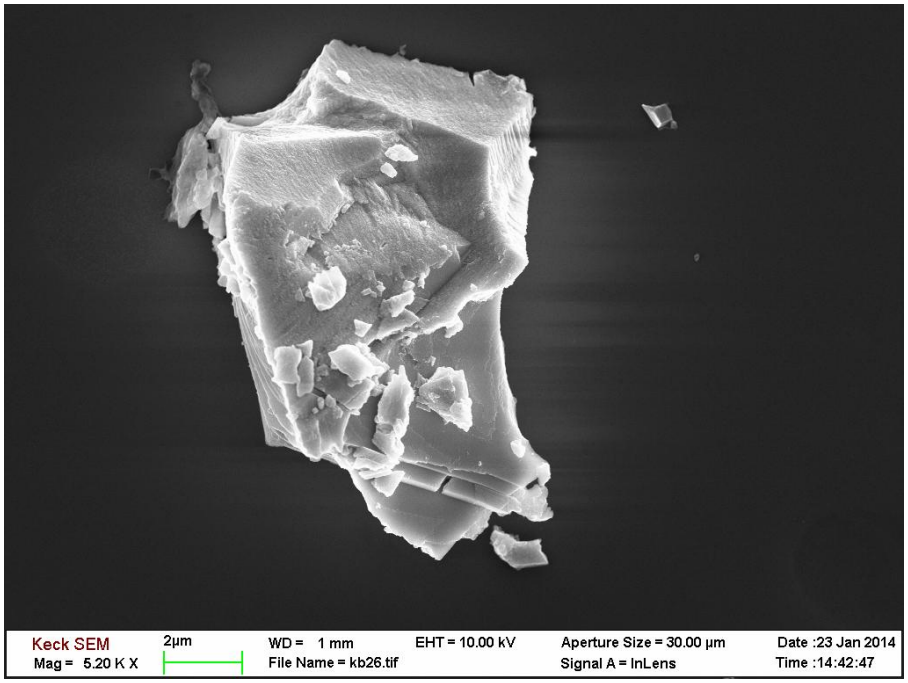

Figure S2 SEM image of the supercrystal grain with sharp broken edges, indicating the grain size over 100 microns. Note: some small pieces, caused by the sample handling and transfer, remain on the surfaces.

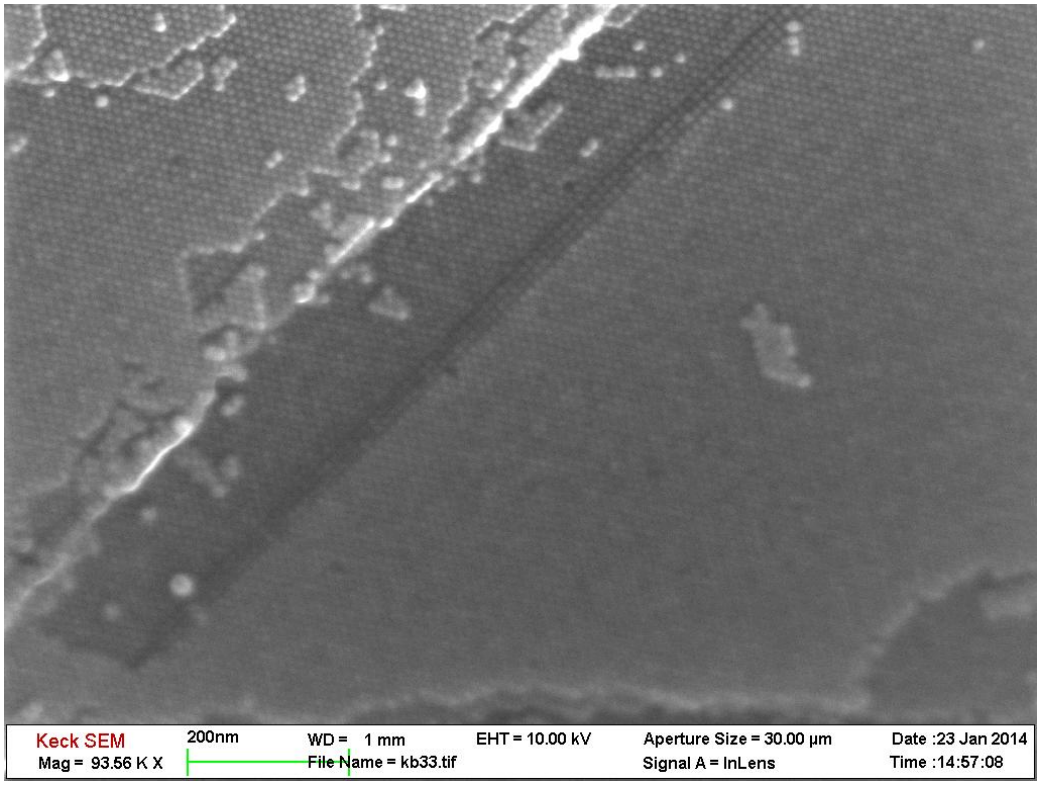

Figure S3 SEM image showing the stacking fault inside the large supercrystal**.**

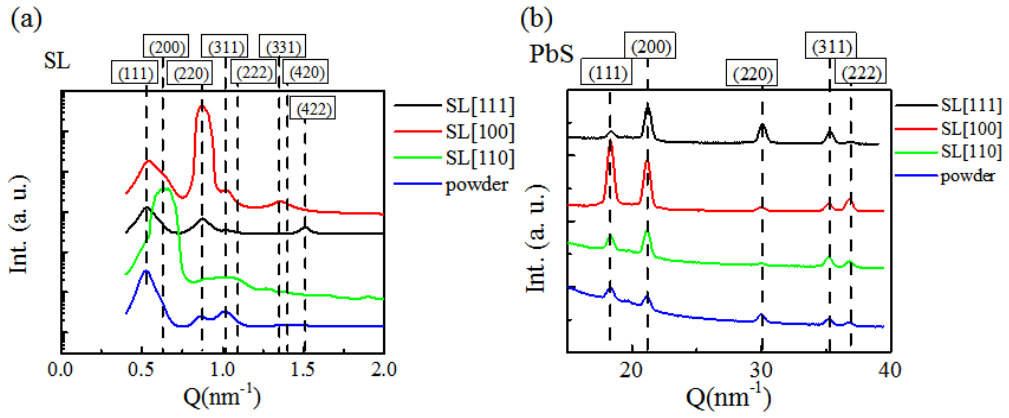

Figure S4 Integrated plots of SAXS (**a**) and WAXS (**b**) patterns collected from NC powder and various oriented NC-assembled supercrystals Note; the patterns of single crystal along SL[111], SL[100] and SL[110] projection and powder sample are indexed into the *fcc* structure, indicating that rocksalt-type cubic NCs assembles into a face-centred-cubic (*fcc*) superlattice structure.

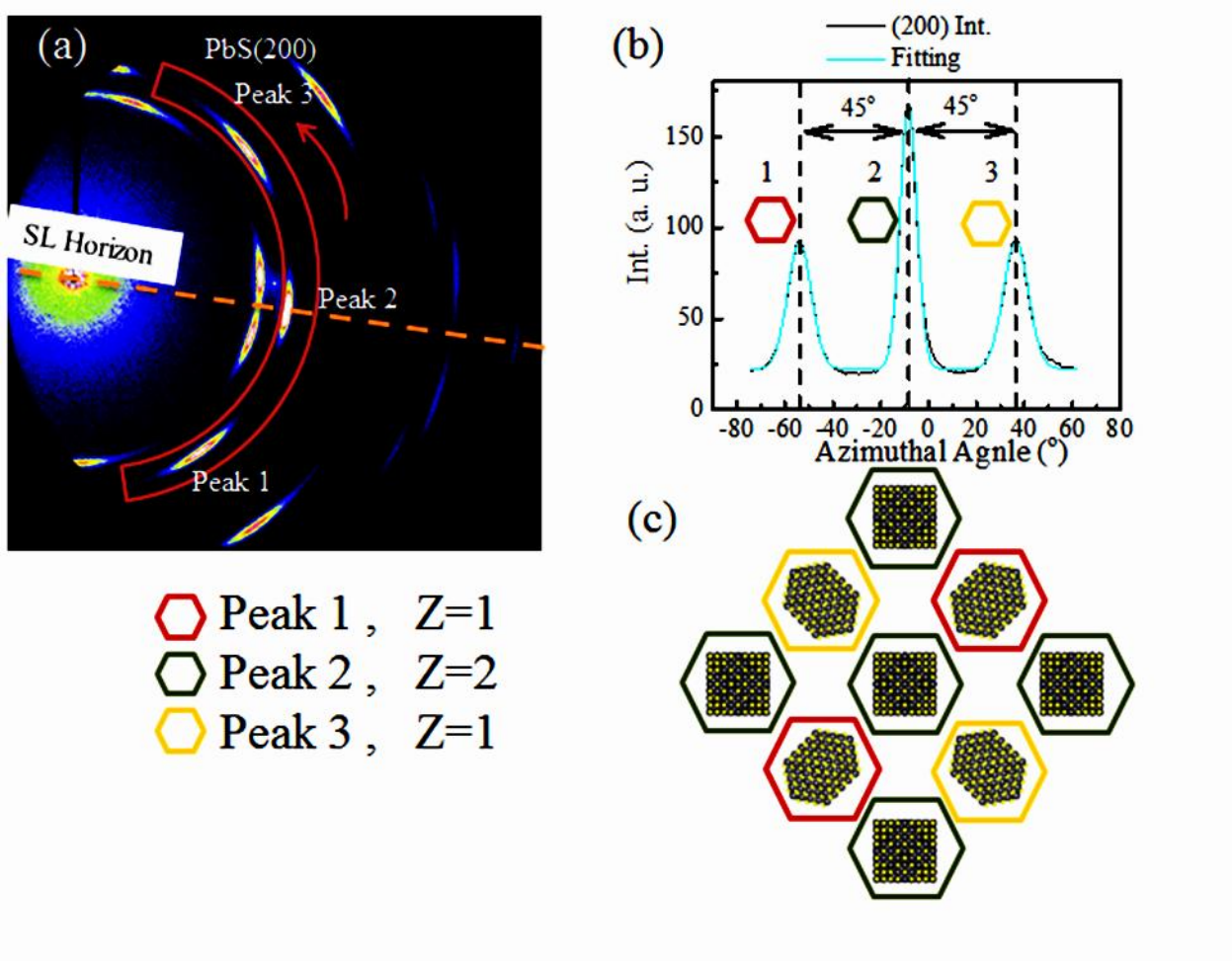

Figure S5 Azimuthal analysis of PbS(200) peaks collected from SL[100] orientation, including (**a**) WAXS pattern with mark of the integration area; (**b**) integration and fitting plot; and (**c**) schematic of NCs with projection on SL(200) plane, showing differently oriented NCs and scattered peaks marked by three colors.

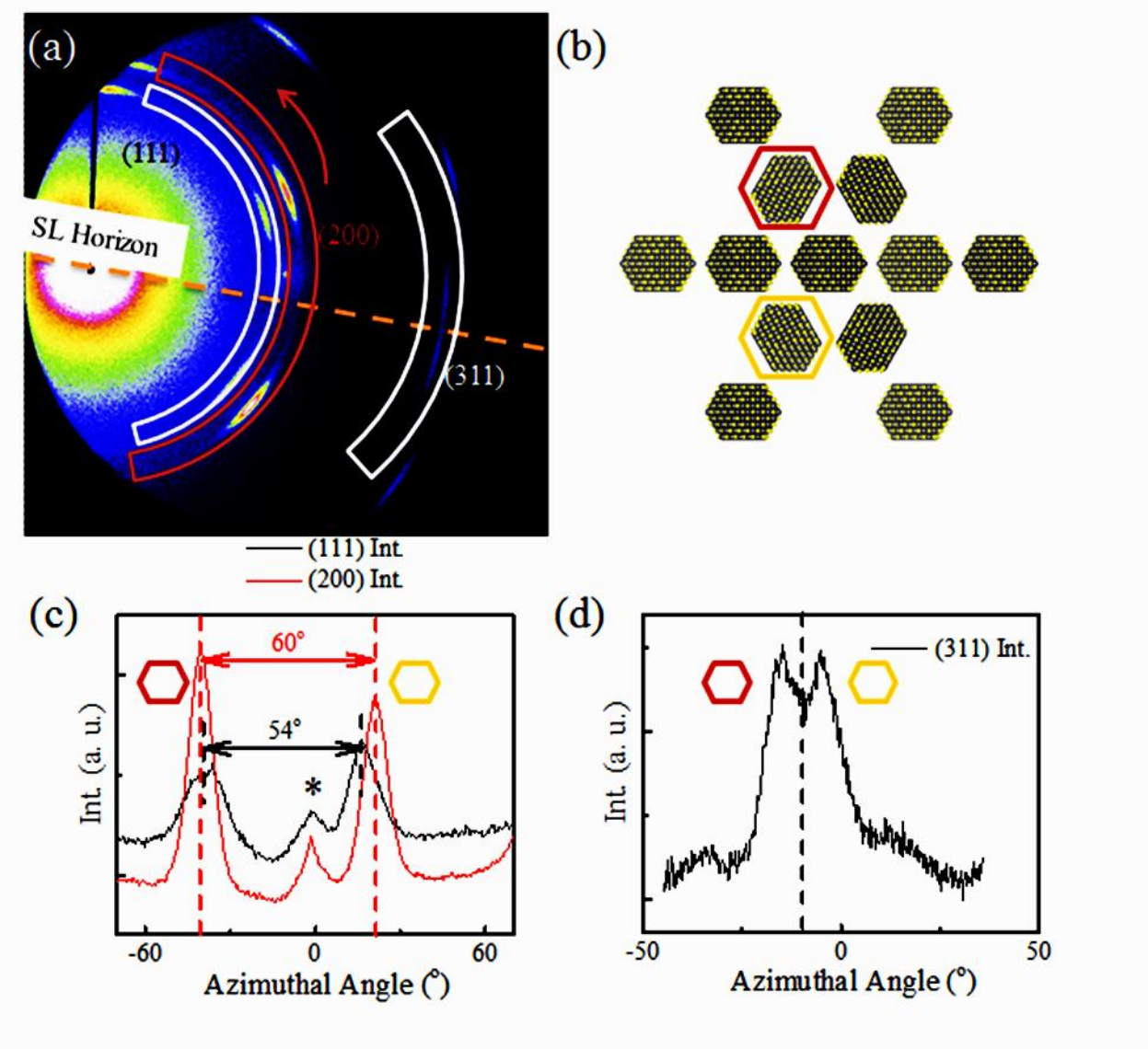

Figure S6 Azimuthal analysis of the scattering peaks collected from SL[111] orientation, including (**a**) WAXS pattern with mark of the integration area, (**b**) schematic of NCs with projection on SL(111) plane and integration plots of (**c**) PbS(111) and PbS(200) and (**d**) PbS (311) peaks. The peak at 0° marked by '*' in (**c**) is the damage-resulted artifact of detector.

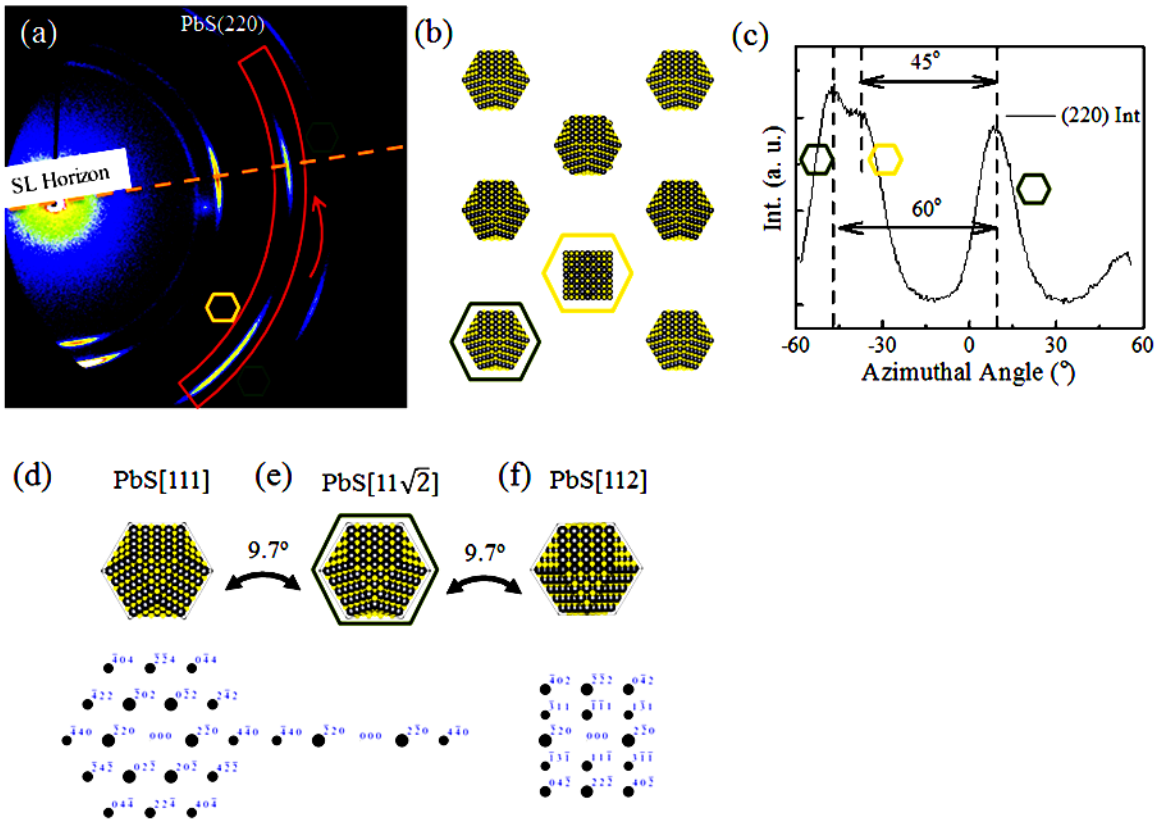

Figure S7. Azimuthal analysis of the scattering peaks from SL[110] orientation, including (**a**) WAXS pattern with mark of the integration area, (**b**) schematic of NCs with projection on SL(110) plane, (**c**) integrated plot of PbS(220) peaks and NCs at corner position (green) and the corresponding simulation images with projections along (**d**) PbS[111], (**e**) PbS[11$\sqrt{2}$] and (**f**) PbS[112].

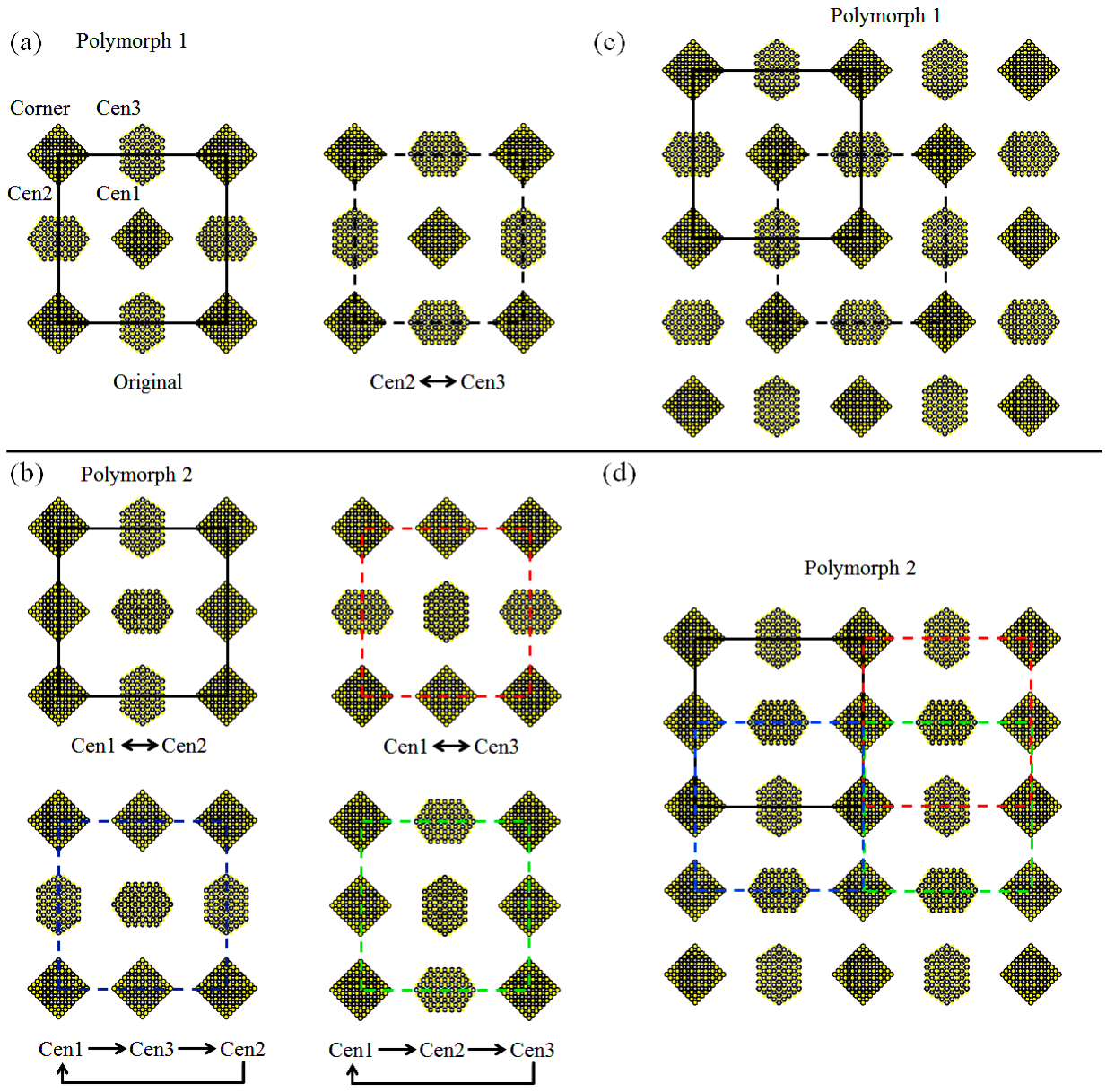

Figure S8. Details for determination and degeneration of superlattice polymorphs with projection of NCs on SL(100) plane. Insets (**a, b**) show six shaped-related superlattice polymorphs determined by position exchange of NCs at three face-center sites. The arrows at bottom show the pathway for position exchange of NCs. Inset (**c, d**) with an expanded 2x2 superlattice cell projected on the SL(100) plane show the degeneration diagrams of two final superlattice pseudo-polymorphs from the originally derived six pseudo-polymorphs: one marked in (**d**) comes from the two original pseudo-polymorphs in (**a**) and another one in (**d**) from four original pseudo-polymorphs (**b**). The lattices marked in solid lines represent the non-

degeneration final pseudo-polymorphs, and the lattices marked in dashed lines represent the starting pseudo-polymorphs.

3. Supporting Tables:

Table S1 Summary of the PbS(200) peaks from SL[100] projected planes.

	Peak1	**Peak2**	**Peak3**	**Peak Ratio**
Peak Position (^{o})	-53.97	-8.45	36.41	
Area	861.26	1273.05	920.13	1.43
FWHM (^{o})	11.74	8.37	12.43	
Height	68.92	142.94	69.54	2.06

Note: the peak ratio is determined by the equation below:

$$Peak\ ratio = \frac{Peak2}{(Peak1+Peak3)/2}$$

Table S2 Interacting facets between neighboring NCs in two *fcc*-based superlattice pseudo-polymorphs. One unit cell includes 24 direct facet-to-facet contacts from 4 truncate NCs. The first two columns show the facets in each polymorph; the last three columns show the facet-to-facet contacts between neighboring NCs. The last column shows the contact numbers of both *trans*- and *cis*-geometry.

Polymorph Number	**{100} Facets**	**{111} Facets**	**{100}‖{100} Contacts**	**{111}‖{100} Contacts**	**{111}‖{111} Contacts (*Trans*- + *Cis*-)**
1	6	8	4	8	12(0+12)
2	6	8	0	16	8 (4+4)

Table S3. Details of the interaction surface facets between neighboring NCs in two *fcc*-based superlattice pseudo-polymorphs, including the type of contacting NCs, the type and number of contacting facets and the geometry in {111}-to-{111} contact. Four truncate NCs in one unit cell include one at corner and three at face-centered sites, marked as Cor and Cen1, Cen2, Cen3, respectively, on projected SL(100) plane. The two contacting facets are from the two neighboring NCs.

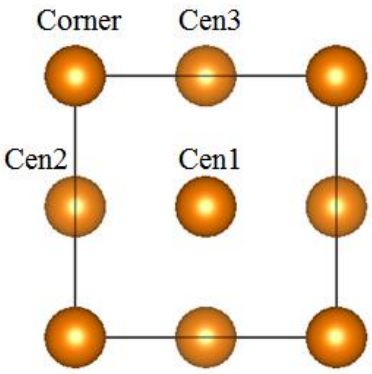

Polymorphs	Contact NCs	Number	Contact Facets	Geometry
1	Cor-Cen1	4	{100}‖{100}	
	Cor-Cen2	4	{111}‖{111}	*cis*
	Cor-Cen3	4	{111}‖{111}	*cis*
	Cen1-Cen2	4	{111}‖{100}	
	Cen1-Cen3	4	{111}‖{100}	
	Cen2-Cen3	4	{111}‖{111}	*cis*
2	Cor-Cen1	4	{100}‖{111}	
	Cor-Cen2	4	{111}‖{111}	*trans*
	Cor-Cen3	4	{111}‖{111}	*cis*
	Cen1-Cen2	4	{100}‖{111}	
	Cen1-Cen3	4	{111}‖{100}	
	Cen2-Cen3	4	{100}‖{111}	

Table S4 Estimation of the packing densities of OA molecules attached at two NC surface facets.

Surface facet of truncate NC	**Pb sites** (atom/nm^2)	**OA density** (using 1/2 Pb sites) (OA/nm^2)	**OA density** (using 1/3 Pb sites) (OA/nm^2)
PbS{100}	5.68	2.84	1.89
PbS{111}	6.55	3.28	2.18
Average	6.12	3.06	2.04